Nanoscale

Accepted Manuscript

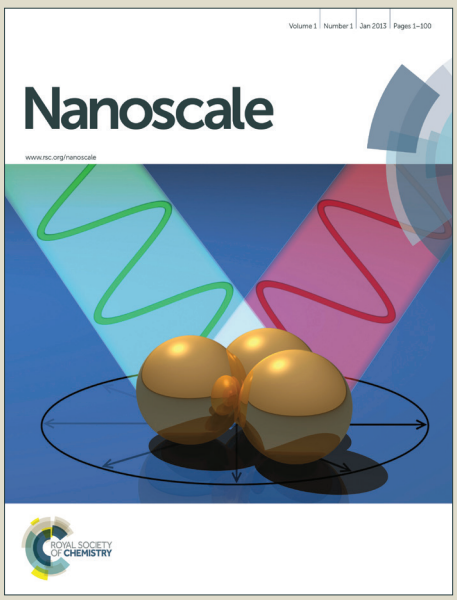

ROYAL SOCIETY OF CHEMISTRY

www.rsc.org/nanoscale

ARTICLE TYPE www. rsc.org/xxxxxx | XXXXXXXX

Direct visualization of N impurity state in dilute GaNAs using scanning tunneling microscopy†

Nobuyuki Ishida,*[a] Masafumi Jo,[a,b] Takaaki Mano,[a] Yoshiki Sakuma,[a] Takeshi Noda,[a] and Daisuke Fujita[a]

Received Xth XXXXXXXXXX 20XX, Accepted Xth XXXXXXXXX 20XX
First published on the web Xth XXXXXXXXXX 200X
DOI: 10.1039/b000000x

Interaction between nitrogen (N) impurity states in III-V compounds plays key roles in controlling optoelectronic properties of the host materials. Here, we use scanning tunneling microscopy to characterize the spatial distribution and electronic properties of N impurity states in dilute GaNAs. We demonstrated that the N impurity states can be directly visualized by taking empty state current images using the multipass scanning method. The N impurity states broadened over several nanometers and exhibited a highly anisotropic distribution with a bowtie-like shape on the GaAs(110) surface, which can be explained by anisotropic propagation of strain along the zigzag chains of Ga and As atoms on the {110} planes. Our experimental findings provide strong insights into a possible role of N impurity states in modifying properties of the host materials.

1 Introduction

Nitrogen (N) doped III-V compounds have attracted attention due to their unique electronic properties, including large band gap reduction [1–7] and emission of extremely narrow band width luminescence from the N impurity center. [8–12] These distinctive properties have been considered to be induced by the interaction between the N impurity states and/or between the N impurity states and electronic states of the host semiconductor. However, the detailed mechanism of the interaction has not been fully understood, and some issues remain controversial from a theoretical point of view. [13–17] One major factor preventing the fundamental understanding is a lack of real space information on the N impurity states.

To date, scanning tunneling microscopy (STM) has been used to provide experimental evidence of spatial distribution of the N impurity states. [18–21] In those studies, most of the STM images were obtained at negative sample voltages (corresponding to filled state images) that showed only localized features of N atoms at substitutional As site. To directly visualize the broadening of the N impurity states, relatively small positive voltages (which provide empty state images) are required since the N impurity states are located close to the conduction band (CB) minimum. [21–23] However, low tunneling conductance at such energy ranges disturbs a stable scanning of a tip over surfaces.

Here, we performed STM measurements on the (110) surface of N-doped GaAs and succeeded in visualizing the broadening of the N impurity states. To image distribution of local density of states (LDOS) at energy ranges where tunneling conductance is low, we employed the multipass scanning method. This method enables empty state current images at around the CB minimum to be provided simultaneously with filled state topographic images. We clarified that the N impurity states were not localized at the impurity site but broadened over several nanometers with a highly anisotropic distribution. The broadening and symmetry of the distribution varied depending on the depth of the N atoms. The origin of the anisotropic distribution is discussed on the basis of the results from a recent density functional theory (DFT) study. [17]

2 Results and Discussion

Figure 1(a) shows a constant-current STM image (topographic image obtained in the first pass, see Methods for details) of the sample around a N-doped layer, acquired with a sample voltage (V_S) of −2.5 V and a tunneling current (I_T) of 100 pA. In addition to the As rows running along the [$\bar{1}$10] direction, [24,25]

† Electronic Supplementary Information (ESI) available: Identification of N impurity positions in terms of depth of depressions in the filled state topographic image. Filled state topographic images of N impurity in fourth plane. Slight modification of topographic height due to existence of N impurity in sixth plane. Current images taken around surface adsorbates. Current and dI/dV images extracted from current imaging tunneling spectroscopy data. Current image of fifth plane N impurity without height correction. Line profiles taken along the [001] and [$\bar{1}$10] for N impurities in first to eighth planes. Differential tunneling conductance spectra obtained above N impurities in first to eighth planes. Position dependence of differential tunneling conductance spectra obtained at N impurity in second plane. Detailed growth conditions of each N-doped GaAs layer.

[a] *National Institute for Materials Science, 1-2-1 Sengen, Tsukuba, Ibaraki 305-0047, Japan; E-mail: ishida.nobuyuki@nims.go.jp*
[b] *RIKEN, The Institute of Physical and Chemical Research, Wako, Saitama 351-0198, Japan*

several N-related features (bright or dark) were observed along the doping layer, as indicated by numbers. The numbers correspond with the atomic layer positions of N atoms below the GaAs(110) surface, where 1 indicates the surface layer. The atomic layer positions of the N atoms were determined with reference to the previous reports[18–20]: dark spots located at the surface As position were identified as the N atoms in the first, third, and fifth planes in terms of the depth of depressions in the topography (see Fig. S1). Second plane N atoms were observed as a kink of the As row. In addition to those features reported so far, we observed the N impurities in the fourth plane. They were imaged as bright or dark features, depending on the tip condition and lateral position at the surface. A typical feature was three bright lines elongated along the [001] direction. The length was about 2.3 nm (four times the lattice constant of GaAs(110) in the [001] direction (a_1)). The separation between the lines was 0.8 nm (twice the lattice constant of GaAs(110) in the [$\bar{1}$10] direction (a_2)), as exemplified in Fig. S2. In addition to the N-related feature, we also observed other features that were difficult to identify, as indicated by R in Fig. 1(a). Those features arise possibly from residual surface contaminants or N atoms at the surface.[18–20]

To directly image the distribution of the N impurity states close to the CB minimum,[21–23] we obtained current images at empty states using the multipass scanning method (see Methods for details), instead of taking empty state topographic images with a conventional constant current mode of operation. Figure 1(b) shows a current image taken at a bias voltage of 1.9 V with a z offset of −100 pm in the second pass. Since the image was obtained simultaneously with the topographic image in Fig. 1(a), the lateral surface positions of those images were identical. At the positions of the N impurities, bright features broadening over several nanometers were observed, in contrast to the localized character (dark spots) in the topographic image. Considering the energy range of the bias voltage, the broadening of those features is considered to reflect spatial distributions of the N impurity states located close to the CB minimum, as discussed later with scanning tunneling spectroscopy (STS) data. These features had highly anisotropic shapes, and the extent of the broadening was dependent on the depth of the impurity position. Discernible changes of the broadening depending on the N composition (within the range from 0.1 to 1 %) was not observed. In the topographic images, the atomic layer positions of N atoms could be precisely determined only for those residing in the first to fifth planes (though slight changes of the topographic signals were also seen for the N atoms below the sixth plane, as shown in Fig. S3). On the other hand, even the N atoms below the sixth plane were clearly imaged in the current images, as exemplified by the one labeled 6 in Fig. 1(b). So far, we have succeeded in identifying the N impurities in up to the eighth plane below the surface (identification of the depth will be discussed in detail later). Although topographic features of the fourth plane impurity at negative voltages showed the variations (bright or dark), the current images at positive voltages exhibited a similar distribution independent of those variations. We also performed imaging at positive voltages (< 3 V) with constant-current mode. However, the tip unexpectedly crashed into the surface at some areas during the scanning. The current images at positive voltages showed that tunneling current was strongly suppressed around some surface adsorbates, as shown in Fig. S4. Thus, the tip is considered to crash when it came closer to such a region.

Strictly speaking, tunneling current at a bias voltage (V) is proportional to the integral of the LDOS of the sample at an energy window between E_F and $E_F + eV$ (E_F is the Fermi level in the sample) weighted by an energy-dependent transmission coefficient.[26] Thus, differential tunneling conductance (dI/dV) is a better signal to be used for imaging distribution of the LDOS at a specific energy since it is directly proportional to the LDOS at an energy (E) with a relationship $E - E_F = eV$. However, when a bias voltage is set around the CB minimum of the GaAs, only the LDOS around there contribute to the tunneling current because the LDOS within the bandgap is zero. As a result, the current images at such energy range are expected to be similar to the corresponding dI/dV images. In fact, we observed similar distributions of the N-induced states between the current and dI/dV images at the voltage range around the CB minimum, as shown in Fig. S5. Since it takes a lot of time to acquire high quality dI/dV images with comparable noise level to the current images, in this work we performed current imaging to characterize the distribution of the N-induced states.

Figures 2(a,b) show a high resolution topographic image ($V_S = -2.5$ V) and corrected current image ($V_S = 1.4$ V) taken around a single N impurity in the fifth plane below the surface. The projected position of the N atom under the surface is marked by a circle, which was determined from the position of the depression in the topographic image.[18–20] To obtain the current image we detected current along the recorded z trace in the first pass (instead of at a constant height), thus the current values were modulated by not only the distribution of the LDOS but also the height corrugation (which follows the As rows in this case since the topography was obtained at a negative voltage). To remove the influence of the height corrugation, we transformed the image to constant height using the well-known form for the dependence of current (I) on tip-sample separation (s),[27]

$$I = I_0 \exp(-2\kappa s), \quad (1)$$

where $\kappa = \sqrt{2m\phi/\hbar^2}$ is the decay constant, determined by the average work function of tip and sample (m: electron mass, $\hbar$: Plank constant). The kappa values measured from I-s curves with our tip and sample were in the range 8-11 nm^{-1}. First,

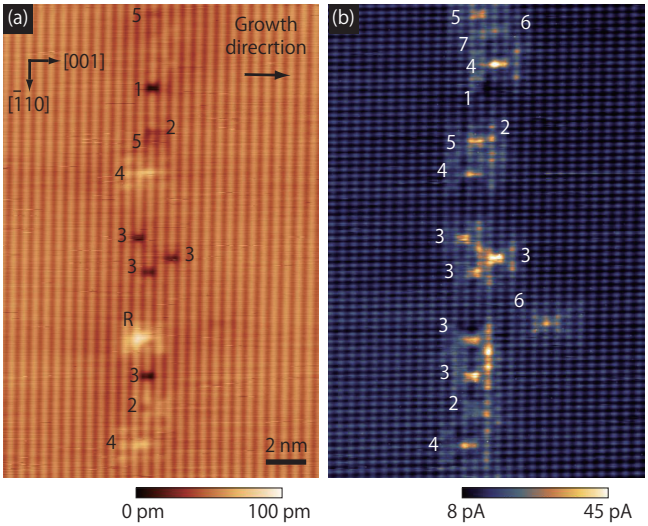

Fig. 1 (a) Constant current topographic image of N-doped GaAs(110) surface obtained at $V_S = -2.5$ V and $I_T = 100$ pA. N-doped layer is clearly identified. (b) Current image ($V_S = 1.9$ V) taken simultaneously with (a) at the identical surface position using the multipass scanning method. N induced features broadening over several nanometers are imaged. The numbers in (a) and (b) correspond with the atomic layer positions of the N below the surface.

we calculated a height difference (Δz) from a reference point at each pixel of the topographic image (here we took the maximum topographic height as a reference). After that, a current value at each pixel in the current image was corrected for by multiplying it by $\exp(-2\kappa\Delta z)$ (Δz has a positive value). We used a value of 10 for κ in Fig. 2(b). Although this compensation method can in principle be applied for an arbitrary STM study using the multipass method, there is one restriction that it has to be used within the range of s where tunneling current shows an exponential dependence. Note that when the tip-sample separation is very small, tunneling current deviates from the exponential dependence[28].

Since the current image reflects the LDOS in the empty states, the round shape features in the image can be correlated with the Ga sub-lattice.[24,25] The N-induced feature was superimposed on the round shape features, showing a highly anisotropic distribution with a bowtie-like shape. The cross sections along the [001] direction between A and A' and along the [$\bar{1}$10] direction between B and B' are shown in Fig. 2(c) and (d), respectively. Dashed horizontal lines show a current value at the Ga-related features of the bare GaAs sites. The N induced feature broadened over ~2.8 nm in the [001] direction ($5a_1$) and ~2 nm in the [$\bar{1}$10] direction ($5a_2$). The center of the broadening was located at the surface As position where the N impurity exists directly underneath (the position of depression in the topography). The edges of the bowtie-like distribution were extended along the four equivalent ⟨112⟩ directions from the center. The distribution was symmetric with respect to the ($\bar{1}$10) mirror plane but slightly asymmetric with respect to the (001) mirror plane. The current values at the right part of the bowtie-like shape were higher than those at the left part [Fig. 2(c)]. Importantly, the magnitude of the κ value (in the range 8-11 nm^{-1}) for the height correction had little effect on those characteristics of the N-induced feature. In addition, the N induced feature in the raw data (without the height correction) also showed the similar characteristics, as shown in Fig. S6. Therefore, we concluded that those characteristics of the N-induced feature were not induced by the effect of height corrugation included in the multipass scanning method.

A recent DFT study by Virkkala *et al.* reported that charge density of the N-induced states propagated along the zigzag chains of Ga and As atoms on the {110} planes (along the 12 equivalent directions) from the N impurity position.[17] On the basis of the theoretical predictions, we will discuss the origin of the anisotropic distribution of the N impurity states observed in the current image. Figure 2(e) and (f) schematically depict the charge density components traveling along the 12 equivalent directions, viewed along the [$\bar{1}$10] and [110] directions (side and top view of the GaAs(110) surface), respectively. An N atom resides in the fifth plane, and the charge density components are depicted by arrows on the ball-stick model of the GaAs lattice. In the side view [Fig. 2(e)], five components (8-12) propagate downward (toward the bulk directions). Note that the components at an angle include two superimposed components. Component 10 propagates along the [$\bar{1}$10] direction, and the other four components travel along the ⟨112⟩ directions in the side view. Components 6 and 7 propagate along the vertical direction to the sheet (the [$\bar{1}$10] and [110] directions) and thus appear as localized features in the side view. Toward the surface directions (upward directions), five components (1-5) exhibit a symmetrical distribution to the components going toward the bulk directions (8-12) with respect to the (110) mirror plane. Since STM is a surface sensitive technique, only the components that reach the surface are expected to be imaged in the experiments. Therefore, we depict the projection of components 1-5 in Fig. 2(e) to the top view of the GaAs(110) surface in Fig. 2(f). Component 3 is localized at the projected N position, and the other four components (1, 2, 4, and 5) propagate along the four equivalent ⟨112⟩ directions in the top view, exhibiting a cross-like shape. The feature broadens over ~2.3 nm in the [001] direction ($4a_1$) and ~2 nm in the [$\bar{1}$10] direction ($5a_2$). The distribution is symmetric with respect to the ($\bar{1}$10) mirror plane but asymmetric with respect to the (001) mirror plane due to the asymmetry of the crystal structure.

The distribution of the N impurity states in the current image in Fig. 2(b) is very consistent with the features of the

charge density components discussed in Fig. 2(e,f): (i) the center part of the distribution was imaged as a bright spot (consistent with component 3 in the model), (ii) the edges of the bowtie-like distribution coincide with the lines of the cross-like feature in Fig. 2(f), (iii) the extent of the broadening in the [001] and [1$\bar{1}$0] directions were comparable with each other, and (iv) the distribution was asymmetric with respect to the (001) mirror plane. On the basis of these findings, we concluded that the N impurity states propagate along the 12 equivalent zigzag directions from the N impurity position as predicted by the DFT calculation.[17] According to the theory, the electronic states induced by the N impurity originate predominantly from the ionic relaxations (strain) propagating along the zigzag chain, initiated by the strong and short Ga-N bonding. Although we found reasonable agreements between the theory and experiment, there are also some slight discrepancies: in the current image, not only the lines of the cross-like shape but also the areas between the lines were imaged bright, showing the bowtie-like distribution. Also, the extension of broadening of the N impurity states to the [00$\bar{1}$] direction (at the left part of the bowtie-like distribution) was slightly larger than that depicted in the model (Fig. 2(f)) by a_1. These findings suggest that the anisotropic strain propagating along the zigzag chains also to some extent affect the ionic relaxations in those regions where we saw discrepancies between the theory and experiment. To analyze the ionic relaxations in detail, description by first-principles calculation is required.

In the current images, we observed several features of the N impurity states, as shown in Fig. 3(a1-a8) (also in Fig. 1(b)). The current images in Fig. 3 were also transformed to constant height in the same way as the one in Fig. 2(b). Those features were distributed differently in size and symmetry: the size increased by a lattice constant of GaAs(110), i.e., 0.565 nm in the [001] direction and 0.4 nm in the [110] direction, step by step from (a2) to (a8), as shown in Fig. S7. The center position alternated between the As site in the first plane and that in the second plane. Although we could not precisely determine the size of broadening in the [1$\bar{1}$0] direction for the image in (a8) [Fig. S7(c8)], it is expected to be $8a_2$ by taking into account the size of broadening in the [001] direction, the center position and the overall shape of the feature. These variations of the distribution can be explained by the difference in atomic layer positions of N atoms, based on the above theoretical model.

Here, we consider the situations where N atoms reside in the first to fourth planes. Figures 3(b1-b4) schematically depict the charge density components that reach the surface in the side view of GaAs(110). The first plane impurity has two components running along the [11$\bar{0}$] and [1$\bar{1}$0] directions at the surface, thus they appear as a localized feature in the side view [Fig. 3(b1)]. These components do not appear at the surface for impurities in other planes, as exemplified in Fig. 2(e)

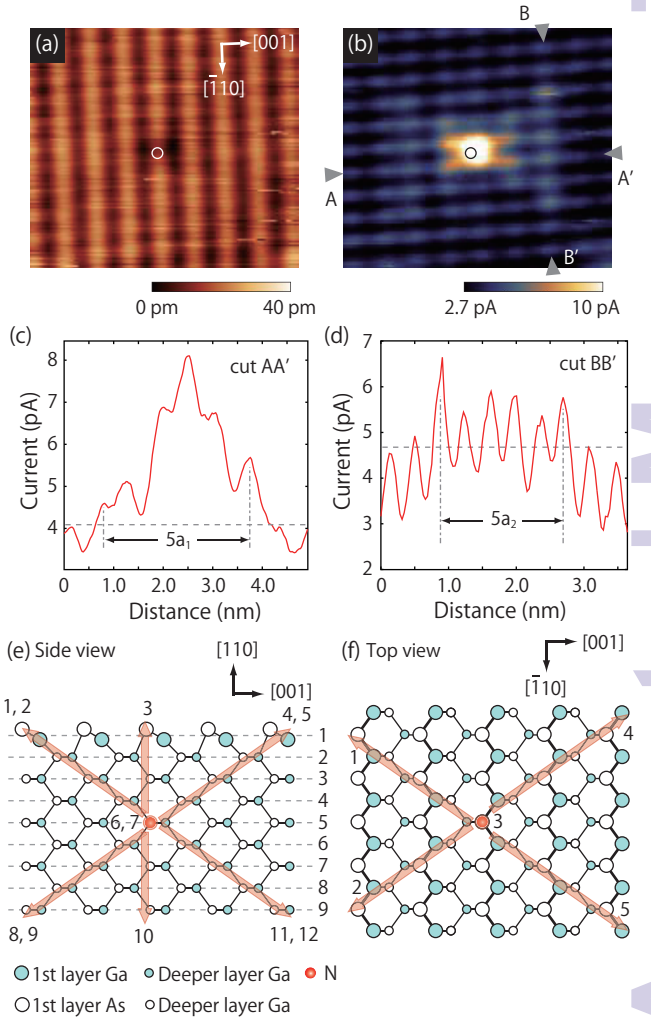

Fig. 2 High resolution (a) topographic image (V_S = −2.5 V) and (b) corrected current image (V_S = 1.4 V) of single N impurity located in the fifth plane below the surface. The projected position of the N atom is indicated by a circle. N atom shows a dark spot localized at the surface As site in (a) but exhibits a bright bowtie-like distribution in (b). (c) and (d) show the cross sections along line AA' and BB' in (b), respectively. (e) and (f) depict the schematic of the propagation of N impurity states from side and top view of GaAs(110), respectively.

(components 6 and 7). In the case of second plane impurity, four tilted components running along the ⟨112⟩ directions in the side view reach the surface [Fig. 3(b2)]. In addition to the four tilted components, the third plane impurity has another component propagating along the [110] direction [Fig. 3(b3)]. For the N impurity below the fourth plane, the charge density has a distribution similar to that of the third plane impurity except for the size of the broadening, as shown in Fig. 3(b4). Figure 3(c1-c4) depict the projections of those charge density components to the top view of the GaAs(110) surface. The first plane impurity exhibits two components traveling parallel to the zigzag chain of Ga and As atoms at the surface [Fig. 3(c1)]. The N impurities below the second plane show the cross-like shape whose size increases in both the [$\bar{1}$10] and [001] directions by a lattice constant of GaAs(110) step by step with the increase in the atomic layer positions [Fig. 3(c2-c4)]. Note that the second plane impurity does not have a localized component at the projected N position due to the missing component traveling along the [110] direction. The center of the distribution alternates between the As site in the first plane and that at the second plane for the odd and even plane impurities, respectively. This leads to a slight difference in symmetry between the odd and even plane impurities. Also, all the cross-like features are symmetric and asymmetric with respect to the ($\bar{1}$10) and (001) mirror planes, respectively.

On the basis of the discussions above, we have determined the atomic layer positions of the N atoms in Fig. 3(a1) to (a8) to be the first to eighth planes, respectively, in terms of size and symmetry of the N impurity states. The projected positions of the N atoms are marked by circles in Fig. 3(a1-a8). The layer numbers determined from the current images agree with those determined from the features in topographic images in the previous reports.[18–20] Also, the distributions in the current images are very consistent with the models in Fig. 3(c1-c4) in many respects: the first plane impurity showed slight increase in the intensity extended to [$\bar{1}$10] and [$\bar{1}$10] directions from the N positions [Fig. S7(c1)]. At the right part of the second impurity feature, two bright spots were observed in the direction of ⟨112⟩ from the N position. At the left part, two components with a weaker intensity were seen in the ⟨112⟩ directions. The intensity difference between the right and left parts provided the asymmetry in the distribution with respect to the (001) mirror plane. Furthermore, the center part of the distribution was imaged dark, which is consistent with the missing component traveling along the [110] direction [Fig. 3(b2) and (c2)]. The N impurity states below the third plane exhibited a bright spot at the position of the projected N atoms and broadened with a bowtie-like shape whose edges travel along the four ⟨112⟩ directions. The current values at the right part of the bowtie-like shape were higher than those at the left part, leading to an asymmetry with respect to the (001) mirror plane, as shown in Fig. S7(b1-b8). So far, we have observed the N impurities residing in up to the eighth plane. This indicates that the N impurity states broaden over at least ~4.5 nm in the [001] direction ($8a_1$) and ~3.2 nm in the [$\bar{1}$10] direction ($8a_2$). The corresponding length of a single component in the radial direction from the N impurity position is about 3.4 nm.

To evaluate the electronic properties of the N impurity states, we performed STS. Figure 4 shows dI/dV-V spectra obtained at the bare GaAs site (averaged over the area including both Ga and As atoms) and above the N impurity sites in the third and sixth planes (at the position of circles in Fig. 3(a3,a6)). During the spectrum measurements, the tip state did not substantially change. In all the spectra, the band gap was observed to be larger than that of the GaAs (~1.5 eV at 78 K) due to the tip-induced band bending.[27,29,30] In the empty states, the spectra obtained above the N sites displayed a peak, as indicated by arrows, while the spectrum at the GaAs site showed no spectral features. The energy position of the peak for the sixth plane impurity is lower than that for the third. These peaks can be identified as arising from the N impurity states since they appeared only in the spectra obtained at the N impurity sites. The energy positions of the peaks were located close to the onset of the dI/dV signals arising from the CB states of GaAs, suggesting that the N impurity states are located close to the CB edge. In fact, this finding is consistent with the previous report.[21–23] Some spectral features were also observed in the filled states at the voltage ranges from −1.7 to −2.3 V. Those features were nearly identical in all the spectra, thus they can be attributed to the surface resonant states of the GaAs(110) surface originating from the As dangling bonds.[25,31] We also performed STS above the N impurity in each plane (at the positions of circles in Fig. 3(a1-a8)), as shown in Fig. S8. Those spectra were obtained at the area with N compositions ranging from 0.1 to 0.3 %. The spectra obtained above the N atoms in the third to eighth planes exhibited peaks around the CB minimum as indicated by arrows while the spectra from the first and second plane impurities did not show distinct spectral features in the empty states though the conductance values were higher than those at the bare GaAs sites. The energy range where the peak features were observed was well coincident with the voltage range we used for the current imaging. This finding suggests that the anisotropic distributions in the current images reflect the broadening of the N impurity states located close to the CB minimum.

In Fig. S8, the energy position and intensity of the peak arising from N impurity states varied among the spectra. The variations can be attributed to the difference in the tip state and/or fluctuation of the surface potential due to the existence of defects, adsorbates, etc. The N impurities in the same plane also showed different spectral shapes for those reasons. However, when the spectra were obtained at the positions close to each other with an identical tip state, the energy position of the peak

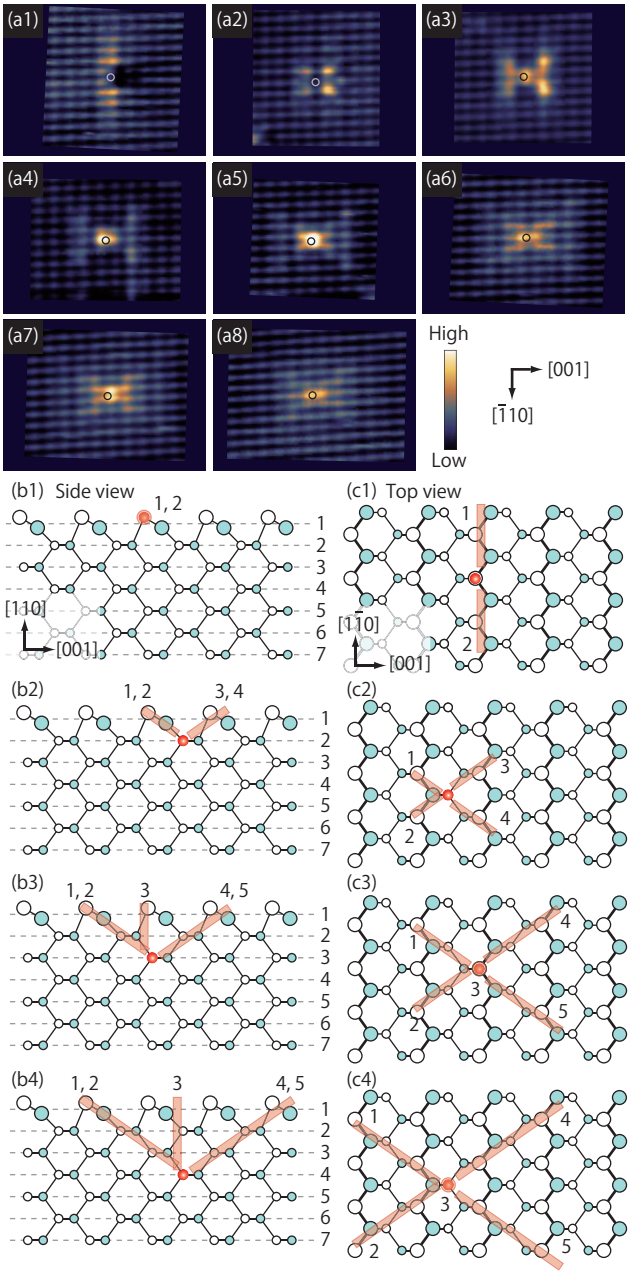

Fig. 3 (a1-a8) Corrected current images of N impurities located in the first to eighth planes. The bias voltages were (a1-a4) 1.8 V and (a5-a8) 1.4 V. Maximum and minimum values of current scale are different in each image. The extent of broadening of the impurity states increases as the atomic layer of the impurities increases. (b1-b8) and (c1-c8) show the schematics of the N impurity states reaching the surface from side and top views of GaAs(110), respectively.

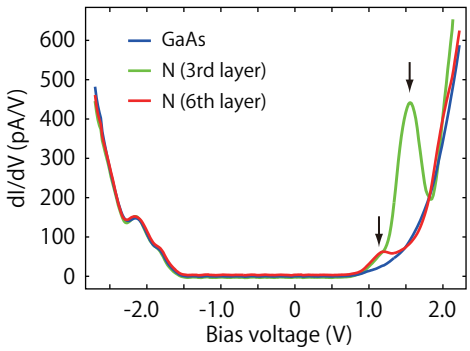

Fig. 4 Differential tunneling conductance spectra obtained at bare GaAs and above N impurities in third and sixth planes.

somewhat correlated with the depth of the impurity position: the peak position shifted to lower energy ranges as the depth increased, as exemplified in Fig. 4. Although we have to confirm the reproducibility for this, a similar tendency was also reproducibly observed in the current imaging measurement: lower bias voltages were needed to visualize the N impurity states in deeper planes. These findings suggest a possibility that the energy position of the N impurity states is correlated with the size of strain, i.e., as the strain becomes weaker along the zigzag chains, the position of the energy states shifts to the lower energy.

Distinct peak features around CB minimum are absent in the spectra for the impurities in the first and second planes [Fig. S8]. One possible reason for this is the missing component of the strain propagation along the [110] direction, as shown in Figs. 3(b1) and (b2). However, distinct spectral features were not observed either, even at the position where the strain propagation components exist. For example, the spectra obtained at the two bright spots in Fig. 3(a2) exhibited only slight shoulder features in the empty states, as shown in Fig. S9. This suggests that relaxation of N-induced strain (which is the predominant cause of the formation of the impurity states) due to the existence of the surface (surface relaxation) plays a key role in reducing the spectral features in the empty states. Since the third plane impurity showed a distinct peak feature in the spectrum, the influence of the surface relaxation is considered to be limited within the first and second planes. In fact, this is consistent with the fact that surface relaxation and resultant change of the bonding configuration occurred only in the first and second layers in the case of GaAs(110)[24,32].

3 Conclusion

We performed STM/STS measurements on dilute GaNAs surfaces. We showed that broadening of the N impurity states

can be directly visualized by taking a current image at empty states. The N impurity states was not localized at the substitutional As site but broadened over several nanometers with a highly anisotropic bowtie-like distribution on the GaAs(110) surface. The anisotropic distribution can be explained by the propagation of strain along the zigzag chains of Ga and As atoms on the {110} planes. We succeeded in identifying the atomic layer positions of N atoms up to the eighth plane from the broadening and symmetry of the distribution of N impurity states. STS measurements suggested that the energy position of the N induced states possibly correlates with the size of strain. Our experimental results provide strong insight into a possible role in modifying the optoelectronic properties of N-doped III-V compounds.

4 Methods

Sample preparation. We fabricated ten N-doped GaAs layers (from layers 1 to 10) with different doping densities on the n-type GaAs(001) substrate by a molecular beam epitaxy. Each N doping was performed in the middle of a 100 nm intrinsic GaAs layer. Active N species were provided by a radio-frequency (rf) N plasma source (ARIOS IRFS-504). The high-purity N_2 gas was fed into the plasma source through a purification filter at a flow rate of 0.06 sccm. The rf power was set at 400 W during the growth supply. The intensity of As_4 flux was 2×10^{-5} Torr beam equivalent pressure. N concentrations in each layer were measured by secondary-ion mass spectrometry. The sheet densities were gradually increased from 4.9×10^{12} to 1.5×10^{14} atoms/cm^2 froms layer 1 to 10. The STM measurements were performed on the layers with doping densities of 1.3 - 2.7 $\times 10^{13}$ atoms/cm^2 (layer 3-5). The volume percentage of N impurities estimated from the STM images was in the range from 0.1 to 1.0 %. The growth conditions in each layer are described in detail in the supplementary information.

STM measurements.

All the measurements were performed at 78 K under the ultrahigh vacuum condition (UHV) ($< 1 \times 10^{-8}$ Pa) with a low temperature STM system (Unisoku USM-1400). Commercial PtIr tips (Unisoku) with a radius of curvature less than 20 nm were used. The tips were heated in UHV by electron bombardment (1 kV, 1 mA) for 1 min and sometimes treated by voltage pulses (around 4 V) in the tunneling regime. An n-type GaAs(001) wafer with N-doped layers on top was cleaved at room temperature to obtain a clean GaAs(110) surface and immediately transferred to the low temperature STM head. A bias voltage was applied to the sample with respect to the tip. In the STS experiments, tunneling current was measured as a function of bias voltage. Differential tunneling conductance spectra (dI/dV-V) were calculated by the numerical derivation of the I-V spectra.

To directly visualize the N impurity states close to the CB minimum, we applied the multipass scanning method[33,34] to current imaging of STM. We used Nanonis SPM control system and the Multipass configuration. In this method, the STM tip scans the same raster line more than twice. In the first pass, topography (z channel) signals are recorded in a constant current mode (conventional STM measurement). In the second pass, the STM tip follows the recorded trace of the z signals in the first pass while the feedback loop is opened. During the second pass, tunneling current at a specific bias voltage is acquired as an imaging signal. A constant offset value can also be added to the recorded z signals (positive values correspond to the so-called lift mode). This method enables visualization of electronic states located even at a low tunneling conductance regime, such as surface states within the band gap of semiconductors. To image the N impurity states, we recorded a topography in the first pass at a relatively large negative voltage (in which tunneling conductance was sufficiently high at all positions of the surface), and a current image was obtained at positive voltages close to the CB minimum in the second pass. In principle, identical current images can also be obtained by using so-called current imaging tunneling spectroscopy (CITS).[26] However, in practice, the multipass method has some advantages over CITS. For example, it enables us to scan a relatively large area (even more than 50 nm $\times$ 50 nm) with a sufficient number of data points (more than 512×512) within a reasonable acquisition time.

5 Acknowledgments

We are grateful to P. Koenraad for advising us on sample preparation. We thank C. Moreno for useful discussions. This work was partly supported by the Mext Program for "Development of Environmental Technology using Nanotechnology" from the Ministry of Education, Culture, Sports, Science and Technology of Japan.

References

1 M. Weyers, M. Sato and H. Ando, *Jpn. J. Appl. Phys.*, 1992, **31**, L853–L855.
2 M. Kondow, K. Uomi, K. Hosomi and T. Mozume, *Jpn. J. Appl. Phys.*, 1994, **33**, L1056–L1058.
3 H. Yaguchi, S. Miyoshi, G. Biwa, M. Kibune, K. Onabe, Y. Shiraki and R. Ito, *J. Cryst. Growth*, 1997, **170**, 353–356.
4 P. J. Klar, H. Grüning, W. Heimbrodt, J. Koch, F. Höhnsdorf, P. M. A. V. W. Stolz and J. Camassel, *Appl. Phys, Lett.*, 2000, **76**, 3439–3441.
5 Y. Zhang, A. Mascarenhas, J. F. Geisz, H. P. Xin and C. W. Tu, *Phys. Rev B*, 2001, **63**, 085205.
6 T. D. Veal, L. F. J. Piper, S. Jollands, B. R. Bennett, P. H. Jefferson, P. A Thomas, C. F. McConville, B. N. Murdin, L. Buckle, G. W. Smith and T. Ashley, *Appl. Phys. Lett.*, 2005, **87**, 132101.
7 T. Mano, M. Jo, K. Mitsuishi, M. Elborg, Y. Sugimoto, T. Noda, Y. Sakuma and K. Sakoda, *Appl. Phys. Express*, 2011, **4**, 125001.

8 T. Kita and O. Wada, *Phys. Rev. B*, 2006, **74**, 035213.
9 M. Ikezawa, Y. Sakuma and Y. Masumoto, *Jpn. J. Appl. Phys.*, 2007, **46**, L871–L873.
10 M. Ikezawa, Y. Sakuma, L. Zhang, Y. Sone, T. Mori, T. Hamano, M. Watanabe, K. Sakoda and Y. Masumoto, *Appl. Phys. Lett.*, 2012, **100**, 042106.
11 M. Jo, T. Mano, T. Kuroda, Y. Sakuma and K. Sakoda, *Appl. Phys. Lett*, 2013, **102**, 062107.
12 M. Jo, T. Mano, Y. Sakuma and K. Sakoda, *J. Appl. Phys.*, 2014, **115**, 123501.
13 S. Sakai, Y. Ueta and Y. Terauchi, *Jpn. J. Appl. Phys.*, 1993, **32**, 4413–4417.
14 W. Shan, W. Walukiewicz, J. W. Ager, E. E. Haller, J. F. Geisz, D. J. Friedman, J. M. Olson and S. R. Kurtz, *Phys. Rev. Lett.*, 1999, **82**, 1221–1224.
15 P. R. C. Kent and A. Zunger, *Phys. Rev. B*, 2001, **64**, 115208.
16 H.-X. Deng, J. Li, S.-S. Li, H. Peng, J.-B. Xia, L.-W. Wang and S.-H. Wei, *Phys. Rev. B*, 2010, **82**, 193204.
17 V. Virkkala, V. Havu, F. Tuomisto, and M. J. Puska, *Phys. Rev. B*, 2013, **88**, 035204.
18 H. A. McKay, R. M. Feenstra, T. Schmidtling and U. W. Pohl, *Appl. Phys. Lett.*, 2001, **78**, 82–84.
19 H. A. McKay, R. M. Feenstra, T. Schmidtling, U. W. Pohl and J. F. Geisz, *J. Vac. Sci. Technol. B*, 2001, **19**, 1644–1649.
20 J. M. Ulloa, P. M. Koenraad and M. Hopkinson, *Appl. Phys. Lett.*, 2008, **93**, 083103.
21 L. Ivanova, H. Eisele, M. P. Vaughan, P. Ebert, A. Lenz, R. Timm, O. Schumann, L. Geelhaar, M. Dähne, S. Fahy, H. Riechert and E. P. O'Reilly, *Phys. Rev. B*, 2010, **82**, 161201(R).
22 D. J. Wolford, J. A. Bradley, K. Fry and J. Thompson, *Proceedings of the 17th International Conference on the Physics of Semiconductors*, Springer, New York, 1985.
23 R. S. Goldman, R. M. Feenstra, B. G. Briner, M. L. O'Steen and R. J. Hauenstein, *Appl. Phys. Lett.*, 1996, **69**, 3698–3700.
24 R. M. Feenstra, J. A. Stroscio, J. Tersoff and A. P. Fein, *Phys. Rev. Lett.*, 1987, **58**, 1192–1195.
25 P. Ebert, B. Engels, P. Richard, K. Schroeder, S. Blugel, C. Domke, M. Heinrich and K. Urban, *Phys. Rev. Lett.*, 1996, **77**, 2997–3000.
26 R. Wiesendanger, *Scanning Probe Microscopy and Spectroscopy*, Cambridge University Press, 1994.
27 R. M. Feenstra, *Phys. Rev. B*, 1994, **50**, 4561–4570.
28 D. Sawada, Y. S. and Ken-ichi Morita, M. Abe and S. Morita1, *Appl. Phys. Lett.*, 2009, **94**, 173117.
29 R. M. Feenstra and J. A. Stroscio, *J. Vac. Sci. Technol. B*, 1987, **5**, 923–929.
30 N. Ishida, K. Sueoka and R. M. Feenstra, *Phys. Rev. B*, 2009, **80**, 075320.
31 C. Pandey, *J. Vac. Sci. Technol.*, 1978, **15**, 440–447.
32 L. Smit, T. E. Derry and J. F. van der Veen, *Surf. Sci.*, 1985, **150**, 245–251.
33 M. Schneiderbauer, D. Wastl and F. J. Giessibl, *Beilstein J. Nanotechnol.*, 2012, **3**, 174–178.
34 C. Moreno, O. Stetsovych, T. K. Shimizu and O. Custance, *Nano Lett.*, 2015, **15**, 2257–2262.